Original Article

Institution of MECHANICAL ENGINEERS

Journal of MECHANICAL ENGINEERING SCIENCE

Proc IMechE Part C:
J Mechanical Engineering Science
2022, Vol. 236(3) 1616–1630

DOI: 10.1177/09544062211013863
journals.sagepub.com/home/pic

SAGE

Effects of interface conditions on heat and mass transfer during modeling of laser dissimilar welding

Zhiyong Li[1,3,4], Gang Yu[1,2,3], Xiuli He[1,3], Shaoxia Li[1], Xu Wang[1,3], Zixun Li[1,3] and Haiming Li[3]

Abstract

An improved 3 D heat and mass transfer model was developed to study the effects of interface conditions during modelling of laser dissimilar welding. In detail, the interface conditions consist of the physical processes at gas/liquid surface (e.g. free surface deformation and optical absorptance), substrate interface (e.g. mixture properties in liquid phase and thermal contact condition) and solid/liquid interface (e.g. fusion line). Their effects on heat and mass transfer are numerically and experimentally analyzed, which are all non-negligible in the welding modelling. In conclusion, free surface deformation influences convection flow and should be considered in the situation of micro-welding and high energy-input welding. Besides, the energy transfer between laser and substrate is more reasonably described by the optical absorptance expressed in polynomial function. The mass transfer induced variation of mixture properties is well described by the method based on time-dependent mixture fraction. Thermal resistance between clamp and substrate should be considered in the modelling of temperature field on macroscale. The joint conductance at substrate interface could be neglected when modelling heat and mass transfer inside the melt pool, while it should be calculated in the simulation of temperature distribution based on the mechanism of heat conduction. The obtained results in this paper provide a vital insight into the interface conditions in laser dissimilar welding process.

Keywords

Laser welding, dissimilar welding, numerical simulation, interface conditions, heat and mass transfer

Date received: 26 November 2020; accepted: 27 March 2021

Introduction

Laser welding is a promising welding technology characterized with high joint quality and high manufacturing efficiency,[1–5] which has been widely studied during the past decades. Dissimilar welding provides great flexibility for engineers and largely decreases the costs, which is also widely used in manufacturing. Consequently, the dissimilar joint achieved by laser welding is widely performed to combine the advantages of laser welding and dissimilar joint. Despite of the strengths mentioned above, there are also many challenges in dissimilar welding such as the formation of unknown intermetallic compounds, liquid cracking and ununiformly mixed elements in melt pool (MP).[6–10] The challenges and problems described above are all mainly affected by the interface conditions during welding process.[11–13] In detail, the interface conditions consist of gas/liquid surface, substrate interface and solid/liquid interface. The illustration of interface conditions and coupled relations are illustrated in Figure 1, and the positions of different interfaces at the melt pool are shown in Figure 2. Many complex phenomena, such as the interaction between laser beam and material (i.e. energy transfer), dominant driving force for fluid

[1]Key Laboratory of Mechanics in Advanced Manufacturing, Institute of Mechanics, Chinese Academy of Sciences, Beijing, China
[2]Center of Materials Science and Optoelectronics Engineering, University of Chinese Academy of Sciences, Beijing, China
[3]School of Engineering Science, University of Chinese Academy of Sciences, Beijing, China
[4]Department of Mechanical Engineering, Northwestern University, Evanston, USA

Corresponding authors:
Gang Yu, Key Laboratory of Mechanics in Advanced Manufacturing, Institute of Mechanics, Chinese Academy of Sciences, Beijing 100190, China.
Email: gyu@imech.ac.cn
Xiuli He, Key Laboratory of Mechanics in Advanced Manufacturing, Institute of Mechanics, Chinese Academy of Sciences, Beijing 100190, China.
Email: xlhe@imech.ac.cn

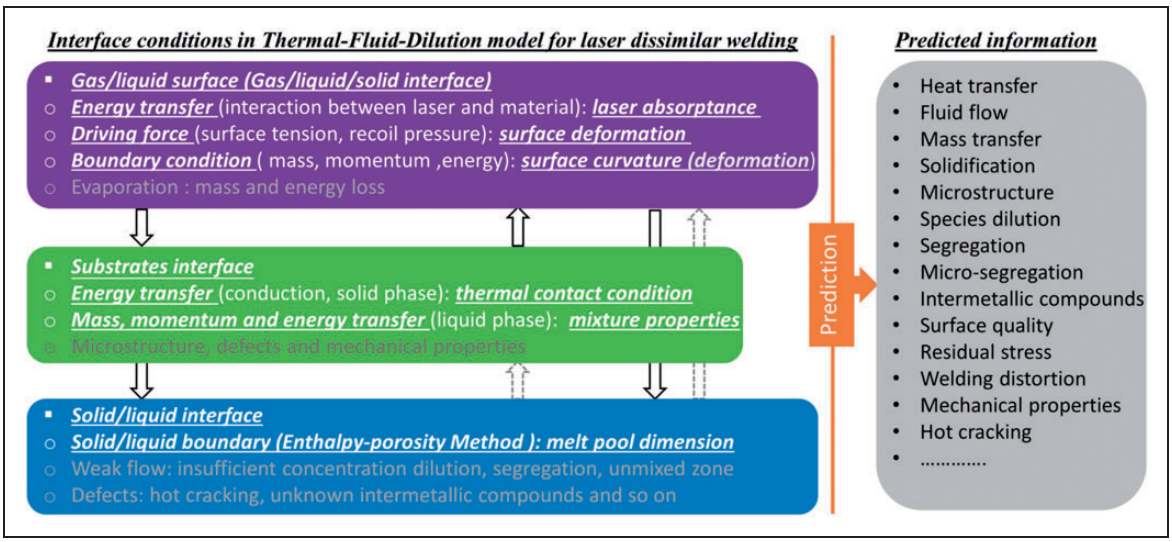

Figure 1. Illustration of interface conditions in laser dissimilar welding and their coupled relations.

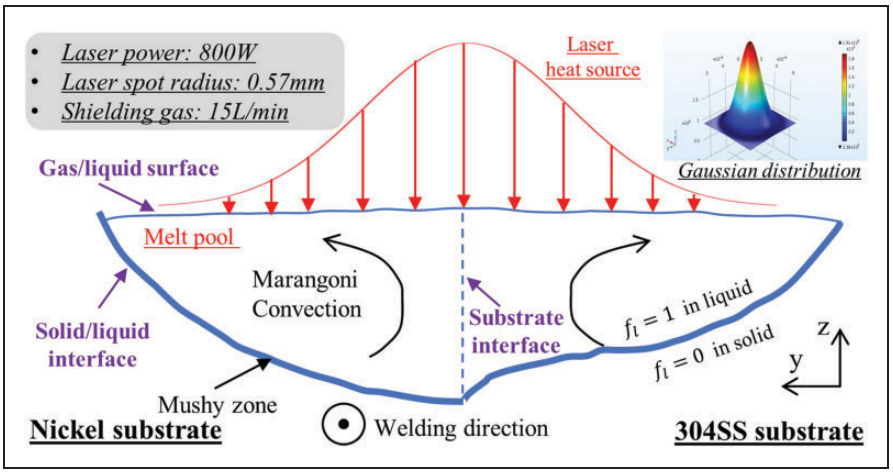

Figure 2. The schematic diagram of melt pool and interface conditions in dissimilar laser welding.

flow (e.g. thermal-capillary force) and metal evaporation (e.g. plasma), are observed at gas/liquid surface. For the substrate interface, mass, momentum and energy are transferred through this interface and the thermal physical properties for different materials experience a sharp change here, and cracking is prone to occurring in this area. Besides, it imposes great challenges for modelling accuracy and convergency and proper treatment for the properties of the mixture is non-negligible. The thermal contact condition at substrate interface should also be paid enough attention because thermal behavior has basic influence on heat and mass transfer. For the solid/liquid interface, the most challenging problem is unmixed zone (UMZ) and still unsolved. UMZ is a small area near solid/liquid boundary where the liquid metal flow is largely restricted and species are nonuniformly diluted, and many defects such as cracking are originated in UMZ. The direct in-situ observation of the interface conditions for the melt pool with high temperature and complex dynamic characteristics imposes great challenges for the experimental observation methods and tools, and thus the numerical method has been developed, which can provide more details in a relatively easier way.[14–15] Here, the laser absorptance which characterizes the energy transfer, gas/liquid surface deformation related to driving force and boundary conditions for fluid flow, properties smooth used to describe the variation of mixture properties at substrate interface, and thermal contact condition for different materials considering the interface thermal transfer are analyzed to study their effects on heat and mass transfer. For the solid/liquid interface, the variation of solid/liquid boundary is analyzed, but the UMZ is only qualitatively discussed and not studied in detail because its mechanism is still not revealed and will be further investigated in future. Additionally, it should be noted that all the interface conditions mentioned above are fully coupled during the whole

welding process, and some decoupled analyses are carried out here only for the better illustration of its effect. The coupled relations are shown in Figure 1, and the full line arrows and dotted line arrows represent the strong coupling and weak coupling, respectively.

The gas/liquid interface of melt pool can be considered as free surface [13,16,17] or flat surface.[18–19] Generally, the melt pool configuration can be predicted more accurately considering the free surface deformation.[20] It is not difficult to understand that the boundary conditions for momentum equation are largely affected by surface curvature and surface tension at gas/liquid interface is proved the main driver for convection flow.[9] As a result, both the heat transfer and fluid flow will be affected. Besides, concentration dilution is mainly driven by convection,[15] thus it is also expected to be affected by the free surface deformation. In several reported works, Esfahani et al.[17] studied the alloy composition and fluid flow during dissimilar welding of carbon steel and stainless steel, and Volume of Fluid method (VOF) was used to capture the surface topography on the gas/liquid surface. The dilution and homogeneity were predicted in their study. Li et al.[13] developed a three-dimensional model to investigate the heat transfer and fluid flow in laser dissimilar welding of 304SS and pure nickel considering the free surface deformation. They used the solidification parameters (e.g., temperature gradient and solidification rate) to predict the morphology in the solidified zone. In this work, the mechanism of the formation of free surface deformation is fundamentally discussed using dimensional analysis method, and its effect on melt pool configuration is numerically and experimentally analyzed.

The laser energy absorptance at gas/liquid surface that characterizes the energy transfer between laser and material is a key parameter and varies with material composition and temperature. A reasonable description of the absorptance is closely related to the transient thermal behavior because the energy for phase change and melt pool development is actually from the energy absorbed from laser.[3,7,8,12] Here, we compare the two relations that can estimate the near-infrared laser energy transfer at gas/liquid interface. One is Hagen-Rubens relation (HR-R),[21] Zhao et al.[22] used it to describe the energy absorptance during laser cladding of T15 powder and T15/CeO2 mixed powder on 42CrMo substrate, and the simulated melt pool configuration and species dilution results match well with the experimental observations. Besides, the high order polynomial relation (HP-R)[23] was used by He et al.[8] in laser spot welding of 304SS to estimate the laser energy absorptance. The numerical model was well validated by the experimental observations, indicating the efficiency of this relation. However, the reasonable explanation for the mechanism of energy transfer between laser and material is still unknown. In this study, these two relations are compared and discussed in dissimilar welding of 304SS and pure nickel under different welding speeds, and then a parametric study of the effect of laser absorptance on temperature field is performed to find a more reasonable relation to describe the energy transfer.

For substrate interfaces, only thermal behavior is considered in solid phase (thermal contact condition), but the mass, momentum and energy are all transferred through this interface in liquid phase when melt pool is formed. The melt pool for dissimilar welding is actually a mixture of liquid metals from different substrates, and its thermal physical properties are actually time-dependent and space-dependent, which imposes great challenges for the development of numerical model and makes it susceptible to many defects.[6,7,13,19] Numerical result is largely affected by the used properties, and it is thus of great importance to reasonably deal with the mixture properties inside the melt pool. There are three commonly used strategies, but no evidence shows which one is more reasonable. Hejripour at al.[20] used the Heaviside function method (HFM) and the volume fraction method (VFM) in the study of mass transfer and solidification in arc welding of dissimilar metals. The simulated MP configuration and concentration fraction were reasonably in agreement with the observed results. Bahrami et al.[18] developed a 3 D FEM model to study the dilution phenomenon during arc spot welding of 1018 steel and nickel, and the dilution rate method (DRM) was used in their model, which had been proved a reasonable method to describe the properties for liquid mixture. To find the most reasonable characterization of the transfer phenomenon at substrate interface corresponding to the real physical process, the simulation studies based on different methods together with experimental validations are all carried out and compared in this investigation.

For dissimilar butt joining, thermal transfer at substrate interface is affected by thermal contact condition. However, it is usually simplified in above models without physical explanation, which has been proved non-negligible in some situations. In the analysis of thermal and mechanical behavior of bolted joint, Fukuoka et al.[24] studied the effect of thermal contact resistance at the interface, and they concluded that it is non-negligible on the calculation of thermal stress. Li et al.[25] developed a FEM model and numerically investigated the effect of thermal contact in thermal resistance welding and results showed that the formation of weld nugget was largely affected by the surface roughness of the electrodes when its value exceeded a threshold. To analyze the effect of thermal contact condition at different interfaces and their effects on thermal behavior, the thermal contact condition at substrate interface and clamp interface (interface clamp and substrate) are separately investigated using both the theoretical analysis and simulation method.

To understand the effects of interface conditions on heat and mass transfer, an improved 3 D heat and mass transfer model was developed considering the free surface deformation and optical absorptance at gas/liquid surface, the property smooth and thermal contact condition at substrate interface, and the melt pool boundary at solid/liquid interface. As shown in Figure 1, the coupled relations and the roles of different interface conditions are illustrated. The contents studied in this work is expressed in white and the content not considered is plotted in gray. Arbitrary Lagrangian Eulerian method (ALE) was introduced to capture gas/liquid surface, and dimensional analysis was also carried out to study the surface deformation. The energy transfer at gas/liquid surface described by laser absorptance were numerically and experimentally analyzed to get the reasonable and accurate characterization. The variation of thermal physical properties for mixed melt pool induced by mass transfer at substrate interface were also studied by using different smooth functions, and the physical mechanism of mixing process through the interface was fundamentally discussed. Finally, thermal contact condition at substrate interface was investigated using both the dimensional analysis and simulation methods. The solid/liquid boundary and its effect on MP solidification are analyzed in the discussion of gas/liquid surface and substrate interface, and not listed in single part. The most challenging and still unsolved problem for interface conditions in laser welding is the UMZ at solid/liquid interface and it will be studied in future based on present work. The effects of interface conditions on heat and mass transfer were summarized in the end to comprehend the physical mechanism of the interaction between laser and materials and get more reasonable simulation results. Fundamental results in this study were worth promoting not only in dissimilar welding but also in other areas, such as additive manufacturing of functionally gradient materials (FGM).

Numerical model

In this work, an improved Thermal-Fluid-Dilution model considering heat transfer, phase change, fluid flow, mass transfer and free surface deformation is developed to study the effects of interface conditions including the free surface deformation and optical absorptance at gas/liquid surface, the smooth method and thermal contact condition at substrate interface, and the melt pool boundary at solid/liquid interface. The simulation domain consists of 304SS substrate and nickel substrate, and the positions of different interfaces are also shown in Figure 2. The chemical composition of 304SS is listed in Table 1. A non-symmetric melt pool is generated under the direct irradiation of high energy density laser beam ($10^8\,W/m^2$).

Fluid flow inside the melt pool is assumed as incompressible laminar flow. The evaporation of the melted material is ignored. The mass density of the material is temperature independent, and the buoyance force is not considered. The governing equations are mass, momentum conservation, energy conservation and dilution, and could be given as follows:

$$\nabla \cdot (\rho \boldsymbol{u}) = 0 \tag{1}$$

$$\rho \frac{\partial \boldsymbol{u}}{\partial t} + \rho(\boldsymbol{u} \cdot \nabla)\boldsymbol{u} = \nabla \cdot (\mu \nabla \boldsymbol{u}) - \nabla \boldsymbol{p} + \rho \boldsymbol{g} - A_{mush}\boldsymbol{u}(1 - f_l)^2 / \left(f_l^3 + M\right) \tag{2}$$

$$\rho C_p \frac{\partial T}{\partial t} + \rho C_p \boldsymbol{u} \cdot \nabla T = \nabla \cdot (K \nabla T) + \rho \frac{\partial (\Delta H)}{\partial t} - \rho \boldsymbol{u} \cdot \nabla (\Delta H) \tag{3}$$

$$\frac{\partial C_i}{\partial t} + \boldsymbol{u} \cdot \nabla C_i = \nabla \cdot (D_i \nabla C_i) + S \tag{4}$$

In relations, ρ is the material density, $\boldsymbol{u}$ and $\boldsymbol{g}$ denote the velocity vector and gravitational acceleration vector, respectively. In addition, μ is the dynamic viscosity, $\boldsymbol{p}$ is the pressure, K is the thermal conductivity and T is the transient temperature inside the melt pool.

Table 1. Concentration of major elements in 304 stainless steel (weight fraction (%).

Fe	Cr	Ni	C	Si
Bal.	18–20	8–10.5	$\leq$ 0.08	$\leq$ 1.8

Table 2. Thermal physical properties used in simulation.[6, 9]

Property	304SS	Nickel
Liquidus temperature (K)	1727	1735
Solidus temperature (K)	1672	1730
Heat of fusion (kJ/kg)	272	290
Specific heat of solid (J/kg·K)	711.3	515
Specific heat of liquid (J/kg·K)	836.8	595
Thermal conductivity of solid (W/m·K)	19.2	60.7
Thermal conductivity of liquid (W/m·K)	50	150
Density of solid metal (kg/m^3)	7450	8900
Density of liquid metal (kg/m^3)	6910	8880
Dynamic viscosity (kg/m·s)	6.70×10^{-3}	3.68×10^{-3}
Surface tension (N/m)	1.872	1.778
Temperature coefficient of surface tension (N/m·K)	-4.30×10^{-4}	-3.40×10^{-4}
Liquid volume thermal expansion (K^{-1})	1.96×10^{-5}	4.50×10^{-5}
Liquid volume concentration expansion	0.078	0.078
Effective mass diffusivity (m^2/s)	7×10^{-7}	7×10^{-7}

f_l is the fraction of liquid phase. The liquid phase fraction is 0 below solidus (T_s) and 1 above liquidus (T_l), and described by $f_l = \frac{T-T_s}{T_l-T_s}$ when the temperature is between solidus and liquidus based on the Carmen-Kozeny relation.[26–27] A_{mush} is a number related to mushy zone morphology and set as $10^7 kg/m^3 \cdot s$. M is a small positive number used to avoid the division by zero and set as 10^{-4}. The dynamic viscosity is 10^5 times larger than the normal value and set as the function of f_l between the solidus/liquidus temperature. In equation (3), C_p is the specific heat and ΔH is the latent heat change caused by phase transition, which is described by $\Delta H = Lf_l$. L is the latent heat of fusion. In equation (4), C_i is the weight fraction of one certain species, and S is the source of the concentration.

The surface tension is described as a traction boundary condition on the free surface. Marangoni effect is considered by the temperature-dependent thermocapillary force. Thermally, the boundary conditions are heat conduction, heat convection and radiation. The initial temperature is 300 K, which is atmosphere temperature. The thermal physical properties used in simulations are shown in Table 2. The thermal physical properties used in simulations are shown in the following table. In this study, laser powder is a constant of 800 W and laser spot radius is 0.57 mm for all the cases.

The PARDISO solver is used to solve all the governing equations based on FEM method, and the domain is discretized by an unstructured mesh. The Arbitrary-Lagrangian-Eulerian (ALE) method[28] is used to describe the free surface deformation. Based on ALE method, the velocity for the mesh at the surface $\boldsymbol{V}_{L/G}$ is described by:

$$\boldsymbol{V}_{L/G} = \boldsymbol{u}_{L/G} \cdot \boldsymbol{n}^* \tag{5}$$

Where $\boldsymbol{u}_{L/G}$ is the velocity of the liquid metal at the gas/liquid interface, and $\boldsymbol{n}^*$ is the unit nominal vector at the surface.

In a typical simulation case in this study, the whole domain is discretized by unstructured tetrahedral mesh, and the maximum mesh size is 80 μm and 400 μm for the fluid domain and solid domain, respectively. The mesh grid consists of 16,039 domain units. The welding time is 100 ms for each study, and the adaptive time step with a maximum size of 0.1 ms is employed. The computation is carried out on the Dell workstation (12×2.5 GHz-24GB). Besides, it should be noted that a mesh-sensitivity test has been performed by varying the mesh sizes before the studies to exclude the effect of mesh discretization.

Results and discussion

Surface deformation at gas/liquid interface

During the dissimilar welding process, shielding gas (15 L/min pure Argon in this study) and surface tension directly act on the gas/liquid surface, and the buoyance force induced by the temperature gradient and concentration gradient acts in the whole MP. In addition, MP dynamics known as Marangoni convection is another non-negligible factor that contributes to the deformation of free surface. Firstly, dimensional analysis method is introduced to investigate the effect of factors mentioned above on the deformation of gas/liquid surface, which provides an important insight to deeply understand its physical mechanism.

Gas/liquid surface is actually the interface for the two-phase flow between shielding gas and liquid metal. To study the relative importance of the effect of shielding gas flow and surface tension on the top surface, Weber number of shielding gas is introduced, and its mathematical expression could be given as follow:

$$We_{Ar} = \rho_{Ar} {V_{Ar}}^2 d/\gamma \tag{6}$$

In which ρ_{Ar} is the density of pure Argon, V_{Ar} is the velocity of shielding gas and d is the diameter of the torch cap. γ is the surface tension coefficient of the MP and assumed as the average value of the surface tension coefficient for 304SS and Ni for simplification. In this study, ρ_{Ar} is 1.784 kg/m^3, V_{Ar} is 2.95 m/s, d is 0.003 m and γ is set as 1.825 N/m. As a result, We_{Ar} is calculated as 0.00865, indicating that the effect of shielding gas flow (pure Argon) could be neglected.

To study the relative importance of the effect of surface tension and melt pool dynamics, Weber number of the melt pool is introduced, and it could be expressed as follow:

$$We_{weld} = \rho_l u_{max}^2 L/\gamma \tag{7}$$

Where ρ_l is the density of mixed liquid metal, u_{max} is the maximum velocity inside the melt pool and L is the characteristic length of the melt pool, which is taken as half of the melt width. In this study, ρ_l is 7895 kg/m^3, u_{max} is 1.23 m/s and L is 0.00073 m. Therefore, We_{weld} is computed to be 3.88, which means that effect of MP dynamics is important, but the effect of surface tension is also comparable.

Besides, based on former study,[9] the fluid flow in the melt pool is mainly driven by surface tension and the effect of buoyance force is negligible. In conclusion, the free surface deformation is mainly caused by surface tension and melt pool dynamics.

Next, the role of gas/liquid surface on melt pool behavior is analyzed, which is expected to be of great significance for melt pool convection. Considering the gas/liquid surface deformation, momentum boundary for convection flow could be expressed as:

$$F_{L/G} = \sigma \boldsymbol{n}^* \kappa - \nabla_s T \frac{d\gamma}{dT} \tag{8}$$

In relations, the right two terms of equation (8) denote the capillary force and the thermocapillary force, respectively. $\boldsymbol{n}^*$ is the unit vector along the normal of free surface, and κ is the curvature of free surface. When flat assumption is applied, κ is thought to be zero. As a result, only the second term at right hand of equation (8) is included when free surface is assumed flat. This is the major difference of momentum boundary, resulting in the differences in thermal behavior, fluid flow and solute dilution. Additionally, capillary force contributes to surface deformation and thermocapillary force dominates Marangoni convection.[10] The fluid flow under the coupled capillary force and thermocapillary force is obviously different from the flow under the single thermocapillary force.

The difference in thermal behavior inside MP could be directly presented by MP morphology. To validate the effect of deformation at gas/liquid surface on MP morphology, MP configurations obtained from experiment and numerical models are compared together under the laser power of 800 W, laser beam radius of 0.57 mm and welding speed of 20 mm/s. As shown in Figure 3, gas/liquid deformation is observed by optical microscope (OM), and free surface captured by ALE method shows great correspondence with the experimental result. It should be noted that the deformation will be more obvious under larger heat input. Though the relatively reasonable result is also simulated by the model based on flat assumption, the difference of the top surface simulated by these two models is obvious. In the simulation of laser micro-welding in which surface quality for weld bead should be considered and laser welding with larger heat input where deformation is more obvious, the accurate capture of free surface is of great significance. What is more, the boundary condition for momentum will also vary with the gas/liquid surface deformation, which has a great effect on heat transfer process inside MP. As shown in Figure 3(b) and (c), the deformation at gas/liquid surface has also affected the MP boundary at solid/liquid interface. To illustrate the effect of MP convection on the curvature of boundary at solid/liquid interface, the Prandtl number, representing the relative thickness of momentum and thermal boundary layers, is introduced and given as follow:

$$Pr = \mu(T)C_p(T)/K(T) \tag{9}$$

If Pr is small, inflexions of the slope of the solid/liquid boundary could be observed due to the competing effects between thermal conduction and convection, while, if Pr is larger, representing that the thickness of momentum layer is much larger, the boundary curvature will be dominated by MP convection.[6]

According to equation (9), the Pr number is also the function of temperature and greatly influenced by the convection flow inside MP. As a result, compared with the experimentally obtained fusion zone in Figure 3(a), the MP boundary (solid/liquid boundary) at solid/liquid interface obtained from ALE model is more reasonable than that obtained from the model based on flat assumption because of the consideration of the deformation at gas/liquid surface. Accurate description of solid/liquid boundary is so important because the direction of max heat flow at any point on solidification interface is normal to this boundary.[5] Competitive growth is observed between easy-growth direction and max heat flow direction for the solidified microstructure, thus, the features of solid/liquid boundary affect the morphology of subsequent grains in fusion zone. Additionally, local solidification velocity is the function of the angle between the laser scanning direction and the normal direction of solid/liquid interface[5] and largely affected by the boundary features. In conclusion, MP boundary at solid/liquid interface is of great importance for MP solidification and also affected by gas/liquid surface morphology.

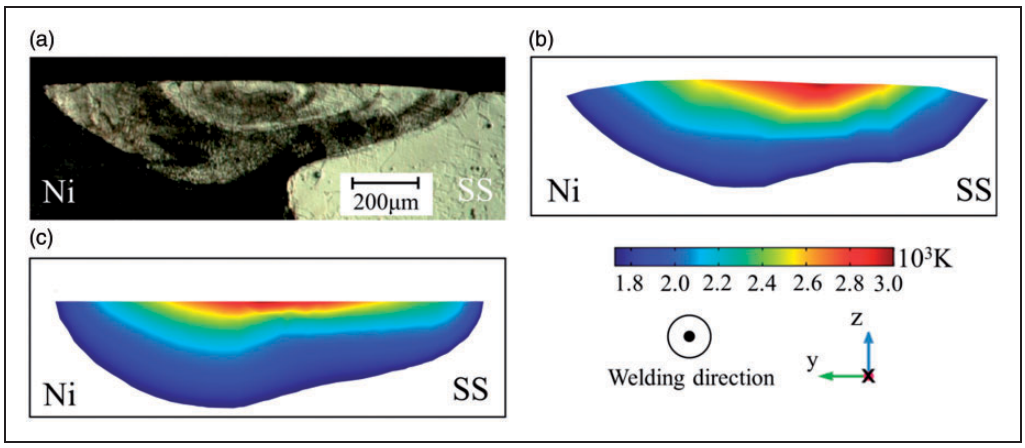

Figure 3. Experimentally and numerically obtained MP configurations. (a) experimental result;[13] (b) simulation result from ALE model; (c) simulation result from the model based on flat surface assumption.

It should be noted that the deformation induced difference of MP morphology is only one aspect of the effect of gas/liquid surface on heat and mass transfer, and further studies on this scope are worth being carried out for reasonable and accurate modelling.

Energy transfer at gas/liquid surface

The energy transfer between laser and material is characterized by laser absorptance, which is temperature-dependent and property-dependent. Energies used for the physical phenomena inside melt pool including phase change and convection flow are all absorbed from laser heat source with high energy density and determined by the transfer condition at gas/liquid surface. Consequently, accurate description of energy transfer contributes to obtaining the reliable simulation results. Based on experimental study and theoretical analysis, there are two functions used to describe the energy transfer at gas/liquid surface considering the change of temperature and material composition. Next, the mechanism and reasonable description of laser energy transfer will be discussed. For simplification, gas/liquid surface is assumed flat in this part.

Hagen-Rubes relation. An estimation of the laser energy transfer between laser and substrates is given by Hagen-Rubes relationship (HR-R),[21] and it could be described as follow:

$$\eta_1(T) = (8\varepsilon_0\omega R_e(T))^{1/2} \tag{10}$$

Where $\eta(T)$ represents the temperature-dependent laser absorptance, ε_0 is the permittivity of free surface and ω is the laser radiation. $R_e(T)$ denotes the temperature-varying electrical resistivity and is assumed to be same for 304SS and Ni for simplification. In this study, its expression is given as:

$$R_e(T) = 1.125 + 1.438 \times 10^{-4}T \tag{11}$$

High order polynomial relation. $\eta(T)$ is related to the laser wavelength and material properties in this situation and described as high order polynomial relation (HP-R).[23] Based on known parameters, the function of $\eta(T)$ is expressed as:

$$\eta_2(T) = 0.365\left(\frac{R_e(T)}{\lambda}\right)^{1/2} - 0.0667\left(\frac{R_e(T)}{\lambda}\right) + 0.06\left(\frac{R_e(T)}{\lambda}\right)^{3/2} \tag{12}$$

In which λ is the wavelength of the laser beam, and the expression of $R_e(T)$ is same as that in HR-R. In this study, the Nd: YAG laser is used as heat source and its wavelength is 1.064 mm.

To get the reasonable characterization of energy transfer at gas/liquid surface, a parametric study on melt width and melt depth is carried out by varying the welding speed from 10 mm/s to 20 mm/s and 30 mm/s. It should be noted that melt pool is asymmetric in dissimilar joining due to the differences of thermal physical properties, and the melt depth changes from 304SS substrate to pure nickel substrate, as illustrated in Figure 3. Particularly, melt pool depth is experimentally and numerically demonstrated larger at nickel substrate,[13] thus the melt pool depth at nickel side is taken as the melt depth for the whole melt pool in this study. As shown in Figure 4, the laser absorptance described in HP-R and HR-R are compared at three different welding speeds. Comparison of the simulated and observed melt pool is commonly used in the calibration of numerical model and of great significance in the modelling of heat and mass transfer inside melt pool.[14,15,18–20] Both the simulated results obtained from HP-R and HR-R show good correspondence with the experimental results with a small relative error, however, the calculated dimension from HP-R is obviously more reasonable than that from HR-R because the error for HP-R is smaller according to the results. Taking the 20 mm/s situation for example, the

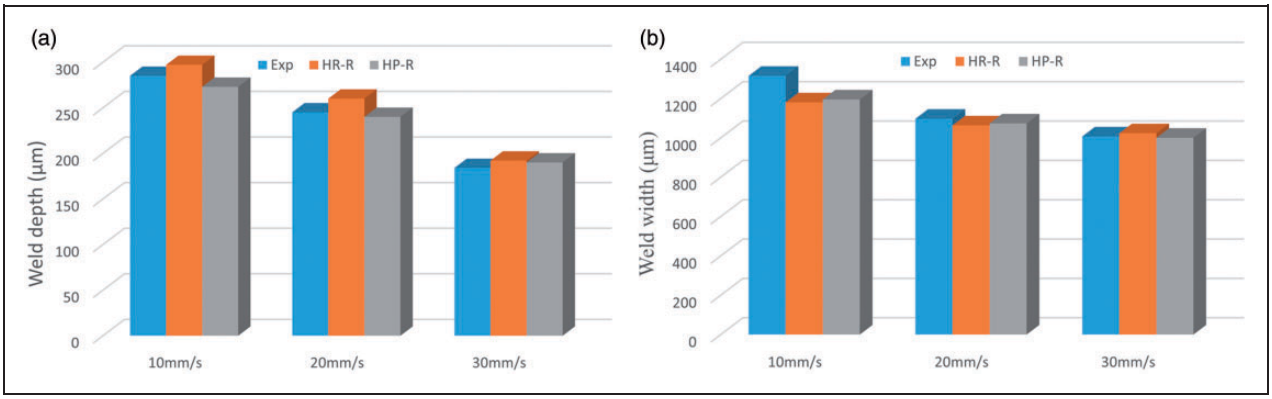

Figure 4. Simulated and experimentally observed MP dimensions at different welding speed. (a) Melt depth; (b) Melt width.

experimentally observed melt width and melt depth are 1097 μm and 245 μm, respectively. The simulated melt width and melt depth are 1063 μm and 260 μm for HR-R, and 1073 μm and 240 μm for HP-R, respectively. Consequently, it could be fundamentally concluded that both HR-R and HP-R are reasonable to characterize the energy transfer between laser beam and substrate material during laser dissimilar welding, however, the error from HP-R is relatively smaller. The interaction between laser and material is a transient and dynamic process, and it is temperature-dependent and property-dependent. When the photon from laser strikes the atom from substrates, phenomena including photoelectric effect and Compton effect are all included. The interaction between photon and atom is a strongly non-linear process and mainly results in the increase of heat energy. Numerical simulation is actually the modelling of energy transfer and the energy transfer induced phase change, convection flow and so on. Therefore, the HP-R with high order polynomial terms describing the strongly non-linear photon-atom interaction is able to provide more reasonable characterization of energy transfer and results in more accurate melt pool dimension.

In addition, for further understanding, the temperature history obtained from HR-R and HP-R at 20 mm/s is plotted together to provide more details. As shown in the sub-figure of Figure 5, the representative point is located at 304SS side and its position is (1.2, -0.3,1) in millimeter at Cartesian coordinates. As illustrated in Figure 5, the peak temperature is around 2650 K for HR-R and 2370 K for HP-R. Obviously, it is much higher in the situation for HR-R. Besides, compared with HP-R, the recorded temperature for HR-R is higher through the whole heating-cooling stage, indicating that more laser energies are absorbed by the substrate in HR-R and then used for the solid-liquid phase change and MP development. As a result, more energies result in larger fusion zone for HR-R, which has been confirmed by the results in Figure 4. With variable parameters, the melt width from HR-P is similar to HP-R, but the melt depth from HR-R is obviously larger. Consequently, based on above discussions, HP-R is a more reasonable description of energy transfer at gas/liquid surface. Besides, it should be noted that the accurate result of thermal behavior is so important and should be paid enough attention because it is closely related to the studies of heat and mass transfer,[29] residual stress[30] and direct simulation of microstructure growth.[31]

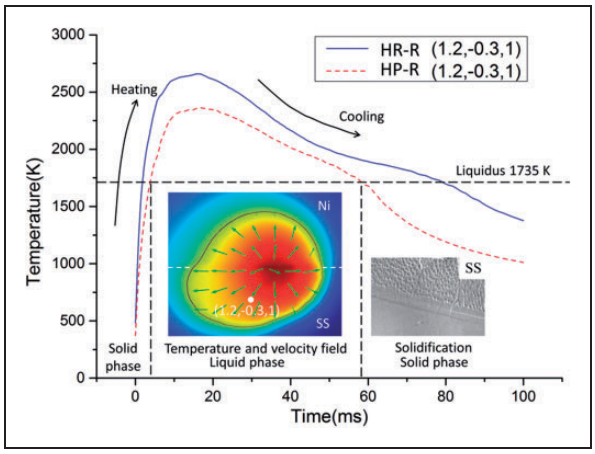

Figure 5. The temperature history for (1.2, -0.3,1) at HR-R and HP-R.

Property smooth at substrate interface

Resulted from the mass transfer through substrate interface in dissimilar welding, the thermal physical properties are time-dependent and change a lot in different positions, which imposes great challenges for the model convergency and simulation accuracy.[9,13,18–20] In liquid phase, mass, momentum and energy are all transferred through substrate interface, thus, an accurate description of thermal physical properties for the mixture is of great importance. In this part, gas/liquid surface is assumed flat and laser absorptance is characterized by high order polynomial relation. Three methods used to describe the mass transfer induced property variation are analyzed to comprehend the transfer mechanism at substrate interface. In detail, they can be expressed as follows:

Volume fraction method. The properties of the mixture inside the MP are calculated based on the volume fraction (dilution) of each substrate, which can be expressed as follow:

$$\bar{M} = \frac{A_{304SS}}{A_{MP}} M_{304SS} + \frac{A_{Nickel}}{A_{MP}} M_{nickel,} \tag{13}$$

$\bar{M}$ represents the mixture properties, which could be represented by density, specific heat, dynamic viscosity and so on, while M_{304SS} and M_{Nickel} are the properties of 304SS and Ni at liquid phase, respectively. Volume fraction of each alloy is assumed equal to the area fraction and calculated based on the area measurement of solidified weld bead. A_{MP} is the total area of the melt pool, and A_{304SS} and $A_{nickel,}$ denote the melted area of the base metals of 304SS and pure nickel, respectively.

Heaviside function method. As illustrated in Figure 6, the properties are temperature-independent and smoothed by Heaviside function with a relatively small scale. Both the solid properties and liquid properties could be characterized in this way. The property used for calculation is also shown in the sub-figure of Figure 6 in a 3 D view.

Dilution rate method. The properties for the MP mixture are set as the function of dilution rate and time

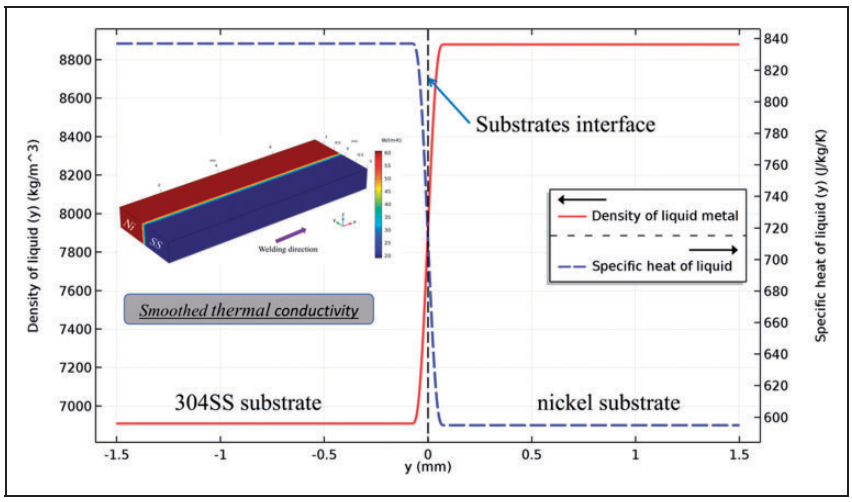

Figure 6. Properties variation described by HFM.

step. As a mixture of melted 304SS and nickel, the properties of the melt pool are assumed to linearly depend on the dilution rate α.

$$\bar{M} = \alpha M_{nickel} + (1-\alpha) M_{304SS} \tag{14}$$

The left hand of Eq. (14) is the physical properties for the mixture, which could be represented by density, surface tension coefficient and so on. M_{304SS} and M_{nickel} denote the physical properties of 304SS and pure nickel in liquid phase, respectively. In DRM, the trend of the property variations resulted from the mixing of liquid metals and its effect on mixture properties are described by the mixture fraction α.[18] According to equation (14), it could be concluded that this trend is same for all the used properties in simulation, such as specific heat and thermal conductivity. The expression of mixture fraction α for the whole melt pool could be obtained from α_i, which could be given by:

$$\alpha_i = \frac{C_i - C_i^{304SS}}{C_i^{nickel} - C_i^{304SS}} \tag{15}$$

Where α_i is the mixture fraction of i_{th} element, C_i is the concentration of certain element at certain position in one time step inside melt pool. Ni element mainly from nickel substrate is taken as the representative element. Besides, C_i^{304SS} is the concentration of Ni at 304 SS substrate and C_i^{nickel} is the concentration of Ni at nickel substrate. C_i^{304SS} and C_i^{nickel} are both constants and equal to the initial values of Ni element at 304SS substrates and pure nickel substrate, respectively. At the right side of equation (15), C_i is the only variable. Averaged by a volume average method, the mixture fraction for the whole melt pool is obtained from α_i, which is denoted by α. Thus, it is only the function of time, not the function of space. For simplification, α is assumed equal for all the elements.

To comprehend the physical process of property variation and its effect on heat and mass transfer, MP configurations obtained from experiments and numerical models based on different methods are compared together under the laser power of 800 W, laser beam radius of 0.57 mm and welding speed of 30 mm/s. As plotted in Figure 7, the result of VFM shows a relatively larger error with the experimental result, indicating that the VFM is not so accurate and will not considered in next section. An averaged volume fraction is used in VFM to get mixture properties, while this averaged fraction is only suitable to the melt pool where dilution is homogenous. Mixing here in high-speed laser welding is nonuniform, thus VFM results in much larger differences in the comparison with experimental observation. Both the result from HFM and DRM show good correspondence with the observed result in the comparison of melt width and melt depth, while the latter result is obviously more accurate, especially in the comparison of MP boundary at solid/liquid interface. The solid/liquid boundary is of great importance for MP solidification and needs reasonable description, which has been detailedly analyzed in Part 3.1. Resulting from the fierce competition of heat transfer boundary layer and fluid flow boundary, the liquid/solid boundary at 304SS side changes a lot and it can be well predicted by the model based on DRM. Heat transfer and fluid flow inside the MP are largely affected by the thermal physical properties of the mixture, and the suitable smooth method should be paid enough attention.[30] The mixture properties seriously depend on the dilution phenomenon, and thus the DRM considering the time-dependent and space-dependent dilution rate shows the most accurate result because it reasonably describes the mass transfer induced property variation. Additionally, temperature and velocity distribution are similar between the results from HFM and DRM, which change a lot in the discussion of laser absorptance related to energy input. Thus, it could be

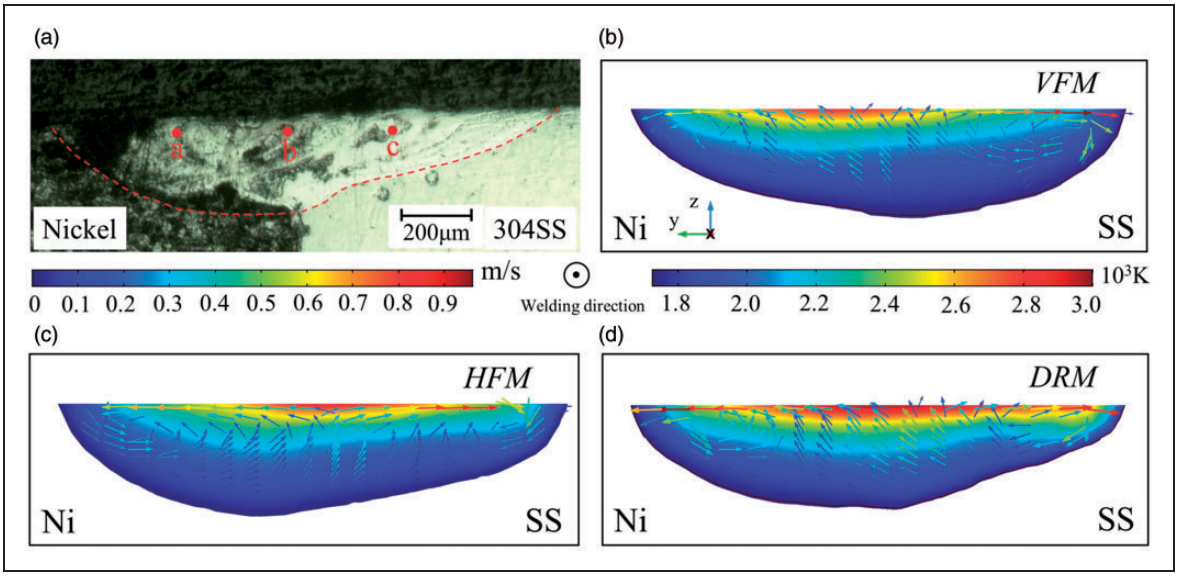

Figure 7. Experimentally and numerically obtained MP configurations. (a) OM observed result; (b) Simulated result from VFM; (c) Simulated result from HFM; (d) Simulated result from DRM.

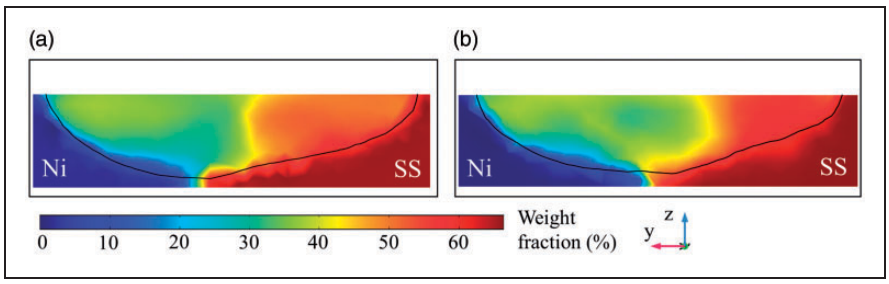

Figure 8. Concentration distribution of Fe element at cross-section of weld bead with different smooth methods. (a) HFM; (b) DRM.

concluded that the simulated temperature and velocity field are prone to being affected by laser absorptance, compared with the property smooth descriptions.

To study the effect of mixture properties on mass transfer, Fe element distribution at cross-section from HFM and DRM are presented in Figure 8(a) and (b), respectively. As illustrated, Fe distribution is not homogenous due to the fast moving of laser heat source and rapid solidification of melt pool, and the calculated result from DRM is obviously more uniform than that from HFM because the spatial variation and time-dependent effect are both taken into account by DRM, which is more consistent with the real physical process occurring in the multi-physics multi-field high-temperature fluid flow.

For further investigation and validation for the mass transfer model, the distribution of Fe element and Ni element is calculated and then compared with EDS result. The positions of three representative points are labeled in Figure 7(a). As illustrated in Table 3, both the results based on HFM and DRM show good correspondence with the EDS result and the relative errors are reasonable, but obviously the DRM result agrees better.

Table 3. Mass fraction (%) of Fe and Ni at three representative points under different smooth methods.

Point	Method	Fe	Ni
a	HFM	37.1	57.8
	DRM	38.3	56.1
	EDS	40.5	51.2
b	HFM	35.0	52.6
	DRM	35.7	49.9
	EDS	43.6	46.5
c	HFM	47.2	37.5
	DRM	49.9	36.0
	EDS	57.8	31.2

The reason why the result based on mixture fraction is more reasonable could be qualitatively explained by the mixing phenomenon inside the MP. Resulting from the movement of laser heat source and quick solidification for laser linear welding, there is continuous melting/solidification process for the MP and concentration dilution is nonhomogenous, as shown in Figure 8 and Table 3. Thus the properties for MP, such as heat conductivity, are also

the function of time and spatial position because it is a mixture of different liquid metals, and this process is reasonably characterized by the mixture fraction inside the MP.

In summary, Volume fraction method (VFM) gives an easier approach to get the mixture properties but presents the largest error because an average volume fraction is used for the whole melt pool in VFM and VFM only works well when dilution inside melt pool is homogenous, which is actually nonuniform for the reasons such as rapid solidification in high-speed laser welding (see Figure 8). For Heaviside function method (HFM), material mixing induced property variations are not considered. Though the property variations at two substrates resulted from phase change could be presented by HFM, the ignoration of material mixing finally leads to the weakness in the predication of solid/liquid boundary (see Figure 7). But, in Dilution rate method (DRM), both the effects of phase change and material mixing on property variations are included, and the time-dependent and space-dependent mixture properties are reasonably characterized. As a result, compared with VFM and HFM, DRM presents the most accurate descriptions of melt pool dimensions and the slopes of solid/liquid boundary.

Thermal contact condition at substrate interface

Resulting from the physical contact, there is thermal contact condition described by thermal contact conductance between different materials. Figure 9 schematically shows the welding system and the position for different interfaces. During the simulation of welding and additive manufacturing in which laser induced melt pool is formed, the thermal transfer at substrate interface is usually ignored in the study of MP behavior and calculation of residual stress without physical explanation. Actually, the validity for this simplification should be physically proved in different situations for reasonable modelling, which is not considered before. In this part, the thermal contact condition at substrate interface and clamp interface, i.e., the surface between clamp and substrate, are considered and studied. Here, gas/liquid interface is flat, laser absorptance is HP-R and property smooth is HFM. Dimensional analysis and numerical simulation both all used for deep understanding of the thermal contact condition and its effect on heat transfer, fluid flow and species dilution.

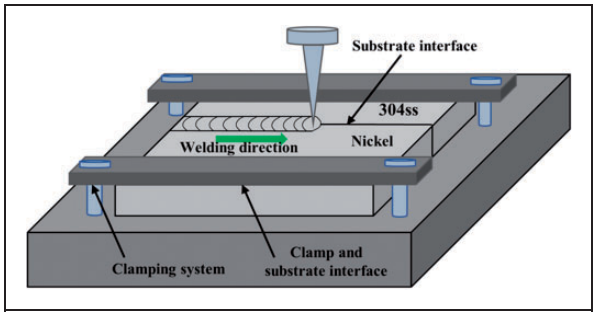

Figure 9. Schematic diagram of the welding system including the illustration of the substrate interface and the clamp interface.

Thermal contact condition at the interface of clamp and substrate (clamp interface). In this situation, the position where the clamp acts is far away from the weld bead, and there is no melting/solidification occurs, as depicted in Figure 9. Thus, the calculation of effective conductance in this area is simplified based on the experimentally obtained function.[24] Heat transfer away from the MP is dominated by the Fourier heat conduction equation, which could be expressed as follow:

$$\rho C_p \frac{\partial T}{\partial t} = \nabla \cdot (K \nabla T) + Q \tag{16}$$

In equation (16), Q is the heat source term and asssumed zero. To estimate the characteristic time for the heat conduction, if the charcteristic length is l, the characteristic time for heat conduction should be:

$$t_h = f\left(\frac{\rho C_p}{K},\ l\right) \tag{17}$$

Taking $\frac{\rho C_p}{K}$ and l as a unit system generates:

$$t_h \approx \frac{\rho C_p l^2}{K} \tag{18}$$

In this study, the charcteristic length l is taken as 40 mm, which is the length of the welding specimens. Therefore, the characteristic time for heat conduction from the M to the clamps at the end of the specimen could be given by:

$$t_{h,Ni} \approx \frac{\rho C_p l^2}{K} = \frac{8900 \times 515 \times 0.04^2}{60.7} = 121s \tag{19}$$

$$t_{h,SS} \approx \frac{\rho C_p l^2}{K} = \frac{7450 \times 711.3 \times 0.04^2}{19.2} = 442s \tag{20}$$

The melting/slidificatoin time for the MP is so small and within several milliseconds. Thus the charateristic time for the MP is at least 4 orders smaller than that for heat conduction at the substrates. In conclusion, the thermal contact condition between the work-piece and clamp has no significant effect on the heat transfer inside the melt pool.

Particularly, in this situation, the thermal contact conductance h_c obtained from experiment is given by:[24]

$$h_c = 10^5 \left[c_1 K \frac{1}{R_a^m} \left(\frac{p}{H_v} \right)^{2/3} + \frac{c_2}{R_a^n} \right] \tag{21}$$

Where K and H_ν are thermal conductivity and Vickers hardness[32] of the contacting solids, respectively, p is the apparent contact pressure and set as 10^5 Pa. R_a is the arithmetic mean of surface roughness of the contact surface and taken as 1.8 μm. Constants of c_1, c_2, m and n are given by 0.006, 0.009, 0.8, and 0.7, respectively.

Based on above boundaries and coefficients, the conductance is taken on the order of 10^6 $W/m^2 \cdot K$, which is non-negligible in the calculation of temperature field of the substrates. For example, for the simulation of residual stress and distortion in laser welding, which is caused by the thermal stress and resistance of macro-movement. Without the consideration of the thermal contact conductance at clamp interface in simulation, heat conduction at substrates is easier. As a result, according to the theory of thermo-elastoplastic mechanics,[12] the modelling results of residual stress and welding deformation are expected to be smaller than the real situation. In addition, clamp interface is so significant to limit the gap between different substrates to a small level. Otherwise, the laser beam with small spot could irradiate through the gap and results in serious defects such as discontinuous welding bead and porosity.[12]

Thermal transfer at substrate interface. With the development of MP, a large proportion of energy is transferred through the substrate interface. As shown in Figure 9, substrate interface is just located at weld bead and the mean temperature here is expected much higher than that at the clamp interface. The joint conductance of the substrate interface between 304SS and nickel, h, has three contributors:[33] the constriction conductance, h_c, forming the contact spots, the gap conductance, h_g, due to the fluid at the interstitial space, and the radiative conductance, h_r:

$$h = h_c + h_g + h_r \tag{22}$$

The Cooper-Mikic-Yovanovich (CMY)[34] correlation is used to calculate the constriction conductance, and it could be expressed as:

$$h_c = 1.25 K_{contact} \frac{m_{asp}}{\sigma_{asp}} \left(\frac{p}{H_c} \right)^{0.95} \tag{23}$$

In equation (23), $K_{contact}$ is harmonic mean of the contacting surface conductivities, σ_{asp} and m_{asp} are the RMS value of the average slope and average height, respectively. p is the contact pressure, and H_c is the microhardness of the softer material.

$K_{contact}$ is calculated to be 29.2 $W/m \cdot K$, m_{asp} and σ_{asp} are 0.4 and 10^{-6} m,[35] respectively. p is set as 10^7 Pa and H_c is the microhardness for pure nickel and it is 160Hv.[7] Consequently, h_c is about $1.3 \times 10^4 W/m^2 \cdot K$.

Based on the parallel-plate gas correlation,[33] the gap conductance, h_g, could be defined as:

$$h_g = \frac{K_{gap}}{Y + M_g} \tag{24}$$

In relations, K_{gap} is the thermal conductivity of air, Y denotes the mean separation thickness, and M_g is the gas parameter, which could be described as:

$$M_g = \alpha \beta \Lambda \tag{25}$$

$$\Lambda = \frac{k T_g}{\sqrt{2} \pi D^2 p_g} \tag{26}$$

Here, α is the thermal accommodation parameter of contact, β is the gas property parameter for air, Λ is the mean free path of gas, k is Boltzmann constant, D is the average particle diameter, p_g is the gas pressure and set as the atmosphere pressure, and T_g is the gap temperature and calculated by:

$$T_g = \frac{T_{SS} + T_{Ni}}{2} \tag{27}$$

The mean separation thickness, Y, is set as zero because the contact pressure p ($10^7 Pa$) is negligible compared with H_c.[33]

The thermal conductivity of air is taken as 0.09 $W/m \cdot K$. α and β are both set as 1.7, and D is 0.37 nm.[35] k and p_g are $1.38064852 \times 10^{-23} J/K$ and 1 atm, respectively. For simplification, T_g is set to be 1000 K. As a result, h_g is calculated to be $1.37 \times 10^5 W/m^2 \cdot K$.

For the situation of high temperature (above 600 °C), such as the simulation of thermal behavior inside the melt pool, the radiative conductance should be considered, and it could be described by the Gray-diffuse plate model:[33]

$$h_r = \frac{\epsilon_{SS} \epsilon_{Ni}}{\epsilon_{SS} + \epsilon_{SS-} \epsilon_{SS} \epsilon_{Ni}} \sigma \left(T_{SS}^3 + T_{SS}^2 T_{Ni} + T_{SS} T_{Ni}^2 + T_{Ni}^3 \right) \tag{28}$$

ϵ_{SS} and ϵ_{Ni} are the emissivity of the 304SS and nickel substrate, respectively. T_{SS} is the temperature for 304SS, and T_{Ni} denotes the temperature for nickel. σ is the Stefan-Boltzmann constant.

For simplification, ϵ_{SS} and ϵ_{Ni} are both set to be 0.2, and T_{SS} and T_{Ni} are considered as 1000 K. Thus,

h_r is calculated to be 25.2 $W/m^2 \cdot K$, and it is obviously negligible.

In conclusion, compared with h_c and h_g, h_r is so small and could be neglected in the analysis of thermal contact condition at substrate interface. For more reasonable illustration, the temperature and flow field, concentration distribution at top surface of the melt pool are all plotted in Figure 10 when the thermal contact condition is considered and when the effect is ignored. In Figure 10, positive x-axis is the welding direction, i.e., the moving direction of laser heat source. For the temperature field, taking the maximum temperature at top surface for example, the difference is only 10 K and the relative error is only 0.34%. As for the velocity field, the relative error is only 1.7%. For concentration dilution, taking the Cr element for example, the distribution for Cr is so similar between two situations. Besides, as shown from Figure 10(a) to (d), the MP dimension decreases a little when the thermal contact condition is considered. Thus, it could be concluded that heat and mass transfer in MP are only lightly affected by substrate interface. Though its effect on heat and mass transfer is negligible, substrate interface should be considered in the modelling of temperature field based on the mechanism of heat conduction considering that the joint conductance is on the order of $10^5 W/m^2 \cdot K$. Besides, effects of substrate interface on the modelling of microstructure, thermal stress, and properties such as fatigue should be paid enough attention because modelling on melt pool scale provides basic information to the simulations focused on other scales, and could be analyzed in future studies. Additionally, the gap should be limited to be small enough and the specific value depends on the specific processing parameters. If the gap is so large, part of the laser beam could irradiate through and results in serious defects including discontinuous weld bead, porosity, and cracking. In this situation, shielding gas cannot absolutely protect the high-temperature melt pool because oxygen and hydrogen from air may enter the gap and react with the liquid metal, which may result in brittle compounds and hydrogen cracking. Besides, it should be noted that the above consideration about the thermal contact condition at substrate interface is only from the aspect of heat transfer process. Actually, complex physical phenomenon such as dynamic flow, species discontinuity at the gap and non-uniform welding distortion due to dissimilar welding will also account for

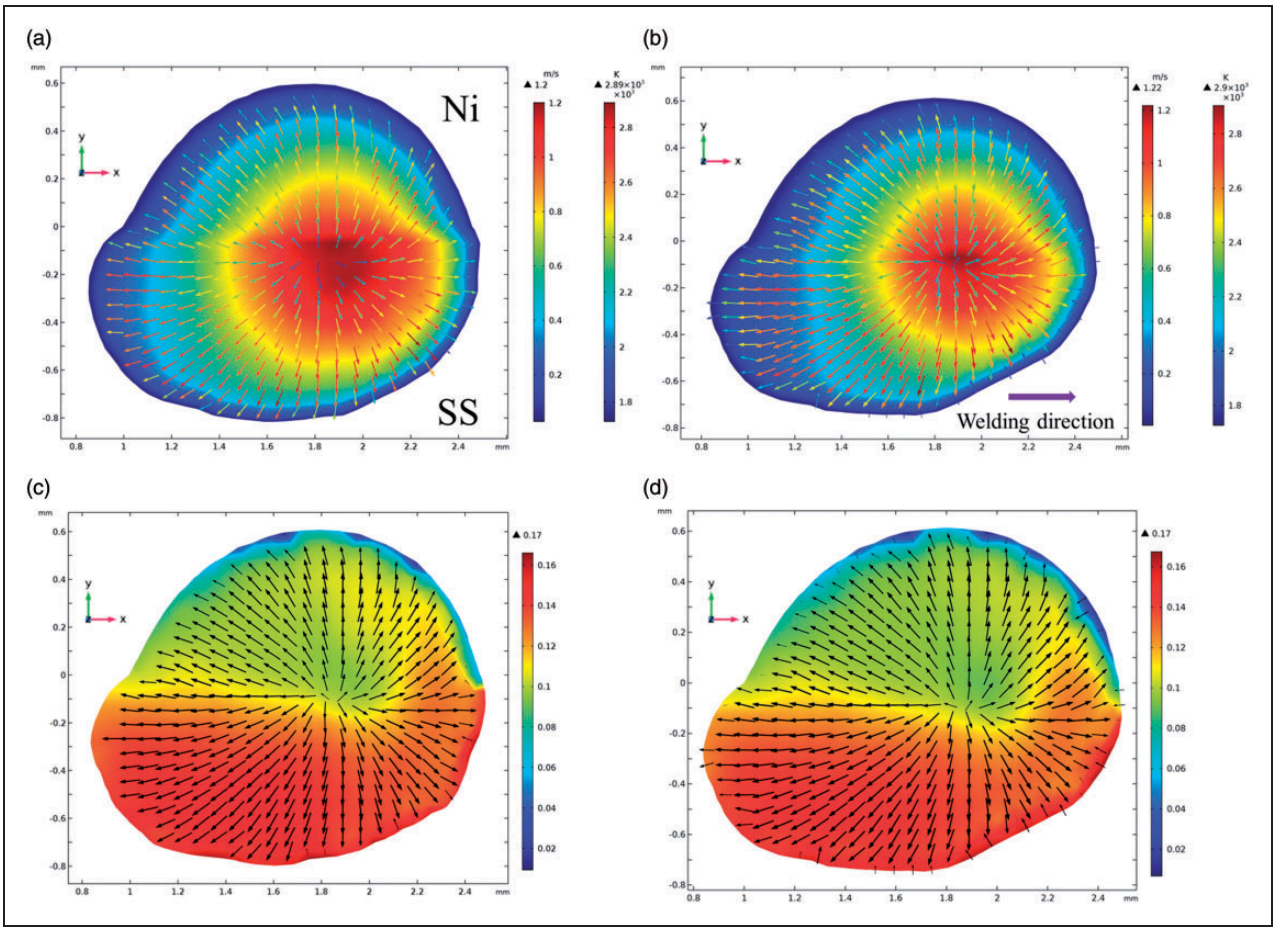

Figure 10. Plot of temperature and velocity field (a) when thermal contact condition is ignored, (b) when thermal contact condition is considered; and distribution of Cr element (c) when thermal contact condition is ignored, (d) when thermal contact condition is considered.

the thermal behavior in the gap. In the future, detailed analysis of the gap and its effect on heat and mass transfer considering above factors will be performed in laser dissimilar welding.

Finally, it should be paid attention that above discussion and conclusions at the analysis of gas/liquid surface, substrate interfaces and solid/liquid interface depend on the developed numerical methods, used processing parameters and adopted material properties to some degree. The results may change a little when different models, methods and materials are used. Anyway, this work provides an important insight into the effects of interface conditions in laser dissimilar joining. Actually, interface conditions including the mass, momentum and energy transfer and sometimes chemical interactions determine the melt pool development, defects formation and then affects the processing quality for many laser manufacturing technologies, such as laser welding, laser drilling and additive manufacturing. More studies on interface conditions should be carried out to reveal the physical mechanism, the relation of process-structure-property, and then achieve parameters optimization, microstructure refinement and quality improvement.

Conclusion

Based on the improved 3 D numerical model, the effects of interface conditions on heat and mass transfer, including studies of the free surface deformation and optical absorptance at gas/liquid surface, the property smooth and thermal contact condition at substrate interface, and the MP boundary at solid/liquid interface are numerically and experimentally analyzed. Some fundamental conclusions could be summarized as follows.

(1) The effect of shielding gas flow on deformation at gas/liquid surface is negligible, and deformation is mainly caused by dynamic flow and surface tension. Both the gas/liquid surface and solid/liquid boundary are largely affected by the deformation of free surface. The major difference in the modelling of heat and mass transfer between flat surface simulation and deformed surface simulation is the momentum boundary, in which coupled capillary force and thermocapillary force, and the single thermocapillary force are considered, respectively. In laser microwelding and welding under high power density, the free surface should be taken into account.

(2) The energy transfer between laser and material at gas/liquid surface is temperature dependent and strong non-linearity. Therefore, the HP-R with high order polynomial terms describing the non-linear relation is able to provide more reasonable characterization of energy transfer and results in more accurate melt pool dimension.

(3) VFM uses an average volume fraction (constant) for the whole melt pool and thus only suitable to describe the mixture properties inside the melt pool when dilution is homogenous. In HFM, only the phase change induced property variations are considered, resulting in the weakness in the predication of solid/liquid boundary. For DRM, both the effects of phase change and material mixing on property variations are included. Based on the reasonable characterizations of time-dependent and space-dependent mixture properties, melt pool dimensions and solid/liquid boundary from HFM are more accurate compared with the results from VFM and HFM.

(4) The thermal contact condition at the clamp surface reaches the order of $10^6\ W/m^2 \cdot K$ and it is negligible in the thermal modelling in melt pool but should be considered in the modelling of residual stress and welding deformation, which would be smaller than the real situation without the consideration of conductance. The joint conductance at substrate interface is on the order of $10^5 W/m \cdot K$ and should be considered in the modelling of temperature field based on the mechanism of heat conduction. Besides, the gap between different substrates should be limited to be small enough to avoid the defects such as discontinuous weld bead, porosity, and cracking.

Highlights

- Mechanism of gas/liquid surface deformation and its effect on MP behavior
- Comparative study of optical absorptance at gas/liquid surface
- Analysis of mass transfer induced temporal and spatial property variation
- Effect of thermal conductance at substrate interface on heat and mass transfer

Authors' Note

Zhiyong Li is working as Visiting Predoctoral Fellow in the Department of Mechanical Engineering, Northwestern University.

Acknowledgments

Zhiyong Li thanks for the help on model development from Dr. Jiaying Gao, Mechanical Department, Northwestern University.

Declaration of Conflicting Interests

The author(s) declared no potential conflicts of interest with respect to the research, authorship, and/or publication of this article.

Funding

The author(s) disclosed receipt of the following financial support for the research, authorship, and/or publication of this article: The authors are grateful for the support from National Natural Science Foundation of China (No.11672304) and the financial help from Beijing Municipal Commission of Science and Technology (Z181100003818015). Zhiyong Li also thanks for the financial help from Chinese Scholarship Council (CSC).

References

1. Mukherjee S, Chakraborty S, Galun R, et al. Transport phenomena in conduction mode laser beam welding of Fe-Al dissimilar couple with ta diffusion barrier. *Int J Heat Mass Tran* 2010; 53: 5274–5282
2. Dong D, Liu Y, Wang L, et al. Microstructure and deformation behavior of laser welded dissimilar dual phase steel joints. *Sci Technol Weld J* 2016; 21: 75–82.
3. Chen G, Liu J, Shu X, et al. Numerical simulation of keyhole morphology and molten pool flow behavior in aluminum alloy electron-beam welding. *Int J Heat Mass Tran* 2019; 138: 879–888.
4. Oliveira JP, Zeng Z, Andrei C, et al. Dissimilar laser welding of super elastic NiTi and CuAlMn shape memory alloys. *Mater Des* 2017; 128: 166–175.
5. Zhiyong L, et al. Fluid flow and solute dilution in laser linear butt joining of 304SS and Ni. *Int J Heat Mass Tran* 2020; 161: 120333.
6. Hu Y, He X, Yu G, et al. Capillary convection in pulsed butt welding of miscible dissimilar couple. *Proc IMechE, Part C: J Mechanical Engineering Science* 2017; 231: 2429–2440.
7. Li Z, Yu G, He X, et al. Numerical and experimental investigations of solidification parameters and mechanical property during laser dissimilar welding. *Metals* 2018; 8: 799.
8. He X, Elmer JW, DebRoy T, et al. Heat transfer and fluid flow in laser microwelding. *J Phys D* 2005; 97: 084909.
9. Li Z, Yu G, He X, et al. Analysis of surface tension driven flow and solidification behavior in laser linear welding of stainless steel. *Opt Laser Technol* 2020; 123: 105914.
10. Hong S, et al. Forming mechanism of bump shape in pulsed laser melting of stainless steel. *Heat Trans* 2017; 139: 062301.
11. Torkamany MJ, Tahamtan S, Sabbaghzadeh J, et al. Dissimilar welding of carbon steel to 5754 aluminum alloy by Nd:YAG pulsed laser. *Mater Des* 2010; 31: 458–465.
12. Kou S. *Welding metallurgy*. 2nd ed. New York: John Wiley & Sons, 2003, p.268.
13. Li Z, Yu G, He X, et al. Study of thermal behavior and solidification characteristics during laser welding of dissimilar metals. *Results Phys* 2019; 12: 1062–1072.
14. Nilanjan C. The effects of turbulence on molten pool transport during melting and solidification processes in continuous conduction mode laser welding of copper–nickel dissimilar couple. *Appl Therm Eng* 2009; 29: 3618–3631.
15. Chen X, Yu G, He X, et al. Numerical study of heat transfer and solute distribution in hybrid laser-MIG welding. *Int J Therm Sci* 2020; 149: 106182.
16. Thompson ME and Szekely J. The transient behavior of weldpools with a deformed free surface. *Int J Heat Mass Tran* 1989; 32: 1007–1019
17. Esfahani MRN, Coupland J, Marimuthu S, et al. Numerical simulation of alloy composition in dissimilar laser welding. *J Mater Proc Technol* 2015; 224: 135–142.
18. Bahrami A, Helenbrook BT, Valentine DT, et al. Fluid flow and mixing in linear GTA welding of dissimilar ferrous alloy. *Int J Heat Mass Tran* 2016; 93: 729–741.
19. Hu Y, He X, Yu G, et al. Experimental and numerical study on laser keyhole welding of 42CrMo under air and argon atmosphere. *Int J Adv Manuf Technol* 2017; 90: 3555–3565.
20. Hejripour F, Helenbrook BT, Valentine DT, et al. Mass transport and solidification phenomenon in dissimilar metals arc welding. *Int J Heat Mass Tran* 2019; 144: 118703.
21. Cohen RW and Abeles B. Efficiency calculations of thermoelectric generators with temperature varying parameters. *J Phys Appl* 1963; 34: 1687–1688.
22. Zhao J, Wang G, Wang X, et al. Multicomponent multiphase modeling of dissimilar laser cladding process with high-speed steel on medium carbon steel. *Int J Heat Mass Transf* 2020; 148: 118990.
23. Bramson MA. Emissivity of various materials. In: William L. Wolfe (eds*) Infrared radiation: a handbook for applications*. US: Springer, 1968, pp. 533–552.
24. Fukuoka T. Finite element analysis of the thermal and mechanical behaviors of a bolted joint. *J Press Vessel Tech* 2005; 127: 402–407.
25. Li YB, Lai XM, Chen GL, et al. The influence of interfacial thermal contact conductance on resistance spot weld nugget formation. *AMR* 2010; 97–101: 3239–3242.
26. Voller V and , Prakash C A fixed grid numerical modelling methodology for convection– diffusion mushy region phase-change problems. *Int J Heat Mass Tran* 1987; 30: 1709–1719.
27. Brent AD, et al. Eethalphy-Porosity technology for modeling convection-diffusion phase change: application to the melting of a pure metal. *Numer Heat Tran* 1988; 13: 297–318.
28. Chan RKC A generalized arbitrary Lagrangian-Eulerian method for incompressible flows with sharp interfaces. *J Comput Phys* 1975; 17: 311–331.
29. He X, Song L, Yu G, et al. Solute transport and composition profile during direct metal deposition with coaxial powder injection. *Appl Sur Sci* 2011; 258: 898–907.
30. Mukherjee T, Zhang W, DebRoy T, et al. An improved prediction of residual stresses and distortion in additive manufacturing. *Comp Mater Sci* 2017; 126: 360–372.
31. Wei HL, Elmer JW, DebRoy T, et al. Crystal growth during keyhole mode laser welding. *Acta Mater* 2017; 133: 10–20.
32. Ross RB *Iron Fe. Metallic materials specification handbook*. Berlin: Springer, 1992, pp.181–197.
33. Adrian B and Allan DK. Thermal spreading and contact resistances. In: *Yovanovich MM and Marotta EE (eds) Heat transfer handboo*k. New York: John Wiley & Sons, 2003, pp. 261–394.
34. COMSOL. Theory for thermal contact. In: Heat transfer module users guide, 2018.
35. COMSOL. Contact switch. In: Heat transfer application library manual, 2018.